Acceleration Sensing Technologies for Severe Mechanical Shock

Anthony Agnello, **Jeffrey Dosch**, **Robert Metz**, **Robert Sill**, and **Patrick Walter**,
PCB Piezotronics, Inc., Depew, New York

Since there is no unique definition of "severe mechanical shock," this article first provides examples of the types of mechanical shock encompassed by this work. Next presented is a summary of lessons learned over the years, and pitfalls discovered, with acceleration sensing technologies used in past measurement attempts of these types of shock. Based on these lessons, a description of current sensing technology approaches and their integration into accelerometers is provided. Due to the uniqueness and severity of some of the shock environments being considered, often the ultimate success or failure of these approaches can only be evaluated in the actual test application. Nevertheless, a descriptor of laboratory evaluation techniques employed during sensor development is provided. Last, results from the application of some of these sensing technologies in actual field applications are illustrated.

The term "severe mechanical shock," as used here, encompasses the gun launch of projectiles and/or projectile barrel exit, high-speed penetration events (earth, rocks, and structures), air blast loading of structures, missile-silo attack, jet engine blade severance, air drop impact, underwater detonation, torpedo impact, transportation vehicle crashes, pile driving, and more. Some subcategories of these shock environments are described in military standards[1] as follows:

Pyroshock – refers to the localized intense mechanical transient response of material caused by the detonation of a pyrotechnic device on adjacent structures. A number of devices are capable of transmitting such intense transients to a material. These devices include explosive bolts, separation nuts, pin pullers and pushers, bolt and cable cutters and pyro-activated operational hardware, flexible linear shape charges (FLSCs), mild detonating fuses (MDFs), explosive transfer lines, V-band (Marmon) clamps, and more.

Gunfire – gunfire environment may be considered to be a high-rate repetitive shock having the form of a substantial transient vibration produced by an air-borne gun muzzle blast pressure wave impinging on the material at the gun firing rate, a structure-borne repetitive shock transmitted through structures connecting the gun mechanism and the materiel, and/or a combination of the two.

Ballistic Shock – is a high-level shock that generally results from the impact of projectiles or ordnance on armored combat vehicles. Armored combat vehicles must survive the shocks resulting from large caliber nonperforating projectile impacts, mine blasts, and overhead artillery attacks, while still retaining their combat mission capabilities. Organizations such as NASA and the Institute of Environmental Science and Technology (IEST) have complementary standards.[2,3]

All of these described environmental inputs to the sensing accelerometer involve various combinations of acceleration levels, velocity changes, and spectral content. These inputs typically occur in more than one direction; however, each accelerometer is intended to isolate and respond to only one vector component of this input. While high-g levels associated with large velocity changes are a challenge, the larger measurement challenge is associated with the combination of high-g levels and broad frequency spectra.

Reference 4 describes the basic physics associated with high-amplitude, broad-spectrum loading of structures. From that document, Figure 1 shows the acceleration time response at the center of a specific, infinite (large-diameter) aluminum plate explosively loaded with TNT. This response would be maintained until relief waves from the plate's edges add complications.

In a real, built-up structure, reflections from joints, interfaces, and interconnections would still further complicate this response. If we assume that an accelerometer responds as a simple, lightly damped oscillator, Figure 2a shows its resonant response to a single impulse. Depending on the relative timing, the accelerometer's response to two similar impulses could be like Figure 2b, which results in near signal cancellation due to a 180-degree, out-of-phase condition. Alternately, if timing were right for three similar impulses, there could be reinforcement as shown in Figure 2c. In short, the amplitude of the response of an accelerometer during the material response phase of a complicated, built-up structure encountering complex or nondeterministic loading is very unpredictable.

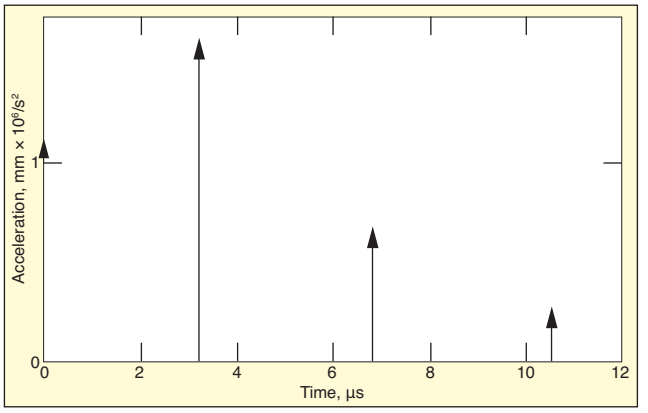

Figure 1. Acceleration versus time of loaded surface of aluminum plate interacting with TNT.

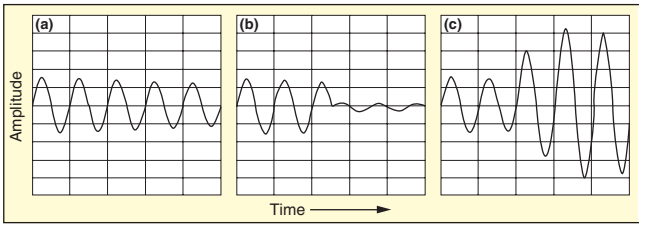

Figure 2. Response of simple spring-mass system to 1, 2, and 3 impulses (a, b and c respectively).

The challenge is then to measure the time-history associated with resulting vibratory modes of the structure, or unit under test (UUT) at the location where the accelerometer is affixed concurrent with or after the material response of the structure has dissipated. This challenge arises because of the unpredictability of the initial response of the accelerometer due to its resonant excitation (see Figure 2) during this material response phase. This initial response will superpose on the UUT's later-time structural response and can cause accelerometer or instrumentation channel over-ranging, problems associated with broad bandwidth input to the analog front portion of the instrumentation system (e.g., slew-rate limiting), accelerometer breakage, and more.

Lessons Learned

A summary of lessons learned in applying various accelerometer technologies to measuring "severe mechanical shock" follows.[4]

The 1950s to mid-1970s. The sensing technology used to measure severe mechanical shock over these decades was almost exclusively piezoelectric-type materials, specifically ferroelectric ceramics. A frequent frustration was that accelerometers containing these ceramics often displayed a baseline shift or offset from their initial zero at shock termination. Reference 5 showed that this shift was an intrinsic property of these ferroelectric ceramics that could

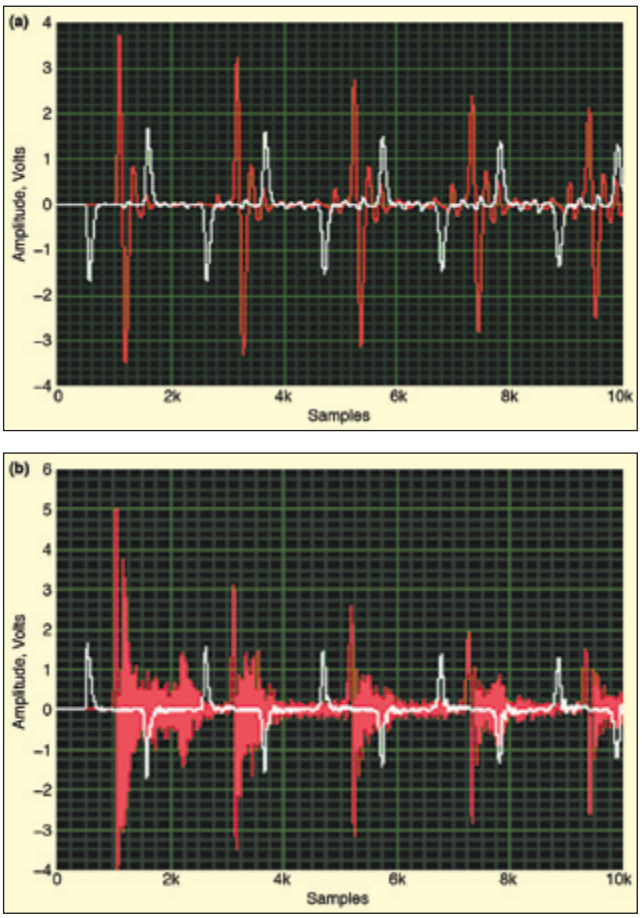

Figure 3. Effect of mechanical isolation on accelerometer response: (a) mechanically isolated; (b) unisolated.

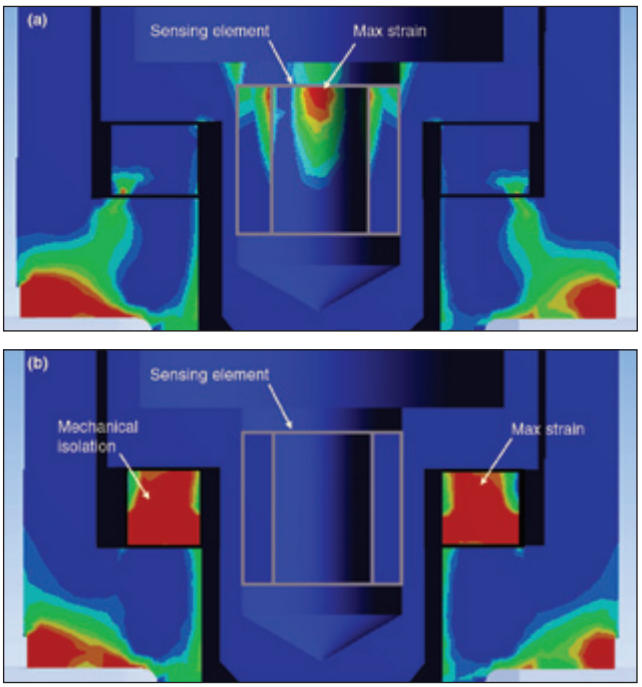

Figure 4. Effect of mechanical isolation on base strain: (a) unisolated; (b) mechanically isolated.

occur at stress levels as low as 100-150 psi.

Mid 1970s to 1983. Discrete semiconductor gages were integrated into accelerometer design (called piezoresistive or PR) for high-g, high-frequency shock. These devices operated on a Wheatstone bridge principal, and the bonded, semiconductor gages themselves were impervious to zero shift. Their small size (about 1 gram) also made them compatible with high-frequency response. An improved sensing and resulting measurement capability in "severe mechanical shock" environments was attained.

1983 to 2010. An all-microelectromechanical (MEMS) sensing technology was integrated into a high-g shock accelerometer (Endevco Model 7270A, B. Wilner) in 1983. Its total silicon flexure, with boron strain gages diffused into the silicon, achieved working ranges to 200,000 g and resonant frequencies to 1.2 MHz. However, loading of the type shown in Figure 1 still excited the resonance of the accelerometer. In addition, with such a wide measurement frequency bandwidth, attention also had to be focused on other modes of vibration (e.g., torsional) of its seismic element that could be excited. Last, its pure silicon flexure, with essentially no damping, resulted in a very high "Q" as compared to ferroelectric ceramic and bonded semiconductor technologies (10 to 20 times higher postulated). So breakage at high frequencies often occurred. In addition, in approximately 1990, attempts began to internally mechanically isolate piezoelectric accelerometers to mitigate mechanical stress input and resulting zero-shift at high frequencies. To lessen the influence of the isolator resonance, these accelerometer designs were typically accompanied by a two-pole filter integrated into the accelerometer housing.

As a by-product of these lessons learned, accelerometer durability and measurement accuracy have improved. The status of current sensing technologies for severe mechanical shock is reported below.

Current Sensing Technologies

Mechanically Isolated and Electrically Filtered Piezoelectrics. It is evident why measurement accuracy is critical when designing piezoelectric accelerometers for severe mechanical shock environments. Durability is further critical because associated issues can cause measurement inaccuracies and even complete data loss in extreme cases.

Mechanical isolation is commonly used with the sensing element (i.e., the piezoelectric ceramic and its attached mass) of an accelerometer to make the accelerometer more durable and less prone to zero shift. The isolator functions as a low-pass mechanical filter decoupling the sensing element from the accelerometer housing at high frequencies. In turn, this protects the element from undesirable, out-of-bandwidth, high frequencies and energy. Figure 3 compares the shock response of an accelerometer both with and without mechanical isolation during a metal-to-metal impact.

Mechanical isolation also reduces the amount of base strain transmitted into the sensing element. Base strain is often the root cause of measurement inaccuracies such as high transverse sensitivity, nonlinearity, and zero shift. It can be defined as any undesired output from the sensing element caused by deformation of the accelerometer's mounting surface. Since base strain can be more of an influence at higher energy levels, both nonlinearity and zero shift become larger error contributors with increasing amplitude. Figure 4 shows a finite-element analysis (FEA) of an accelerometer with and without mechanical isolation. Note how the location of the maximum strain moves off of the sensing element when mechanical isolation is added.

Material properties of the mechanical isolator must be carefully considered, since they can cause additional measurement inaccuracies. Material that is too soft can create linearity issues, because the material will deflect differently at high amplitudes than it does at lower amplitudes. Too soft a material can also result in a sensing system with too low a resonant frequency, negatively affecting the frequency response of the accelerometer below 10 kHz (see Figure 5a). Ten kHz is a minimum design goal in all accelerometers intended to measure severe mechanical shock. Conversely, material that is too hard will not provide enough isolation to reduce the undesired out-of-bandwidth high frequencies and energy.

The cutoff frequency of the isolator must be much lower than the accelerometer resonance to assure adequate high-frequency attenuation. An optimum relationship between stored energy and energy dissipation, or Q factor, for the isolator is desired to maximize the accelerometer's region of flat frequency response. An underdamped system (high Q factor), as shown in red in Figure 6a, will oscillate at its resonant frequency and decay as energy is lost. Figure 6b shows a more optimally damped system.

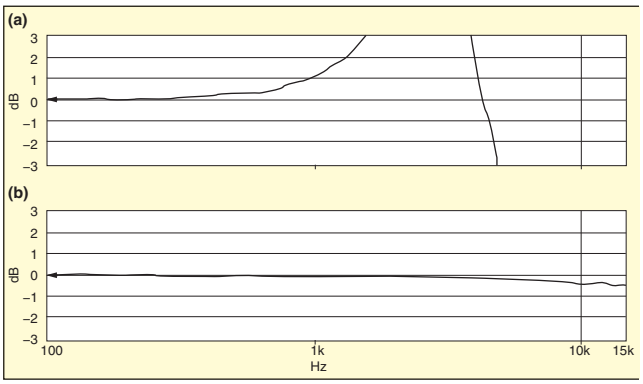

Figure 5. Effect of isolator on accelerometer frequency response: (a) low system resonant frequency; (b) desired frequency response.

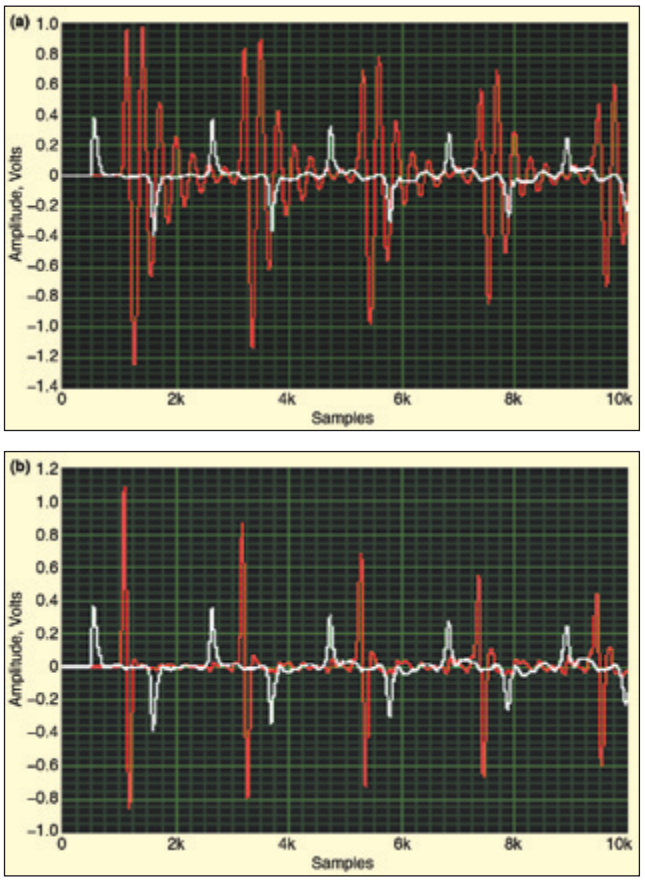

Figure 6. Influence of Q factor of isolator on accelerometer response: (a) under-damped; (b) optimally damped.

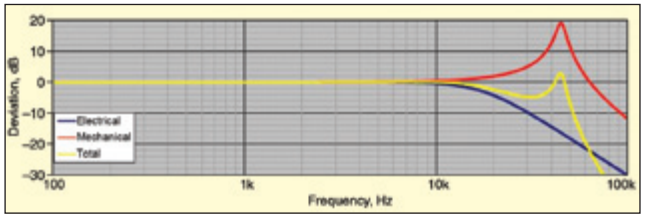

Figure 7. System response of mechanical isolator and electrical filter.

Since optimal damping cannot be attained with a simple elastomeric material, nominal two-pole, low pass electrical filtering is also incorporated in the accelerometer to attenuate any residual resonant peak associated with the isolator. It further eliminates high frequencies and prevents overloading of subsequent signal conditioning. The electrical filter, configured around the ICP® circuit, is tailored to the mechanical isolator's resonant frequency to cause a sensor frequency response that is flat to >10 kHz. Figure 7 shows a representative frequency response function for an accelerometer when the response of the mechanical isolator is combined with an electrical filter.

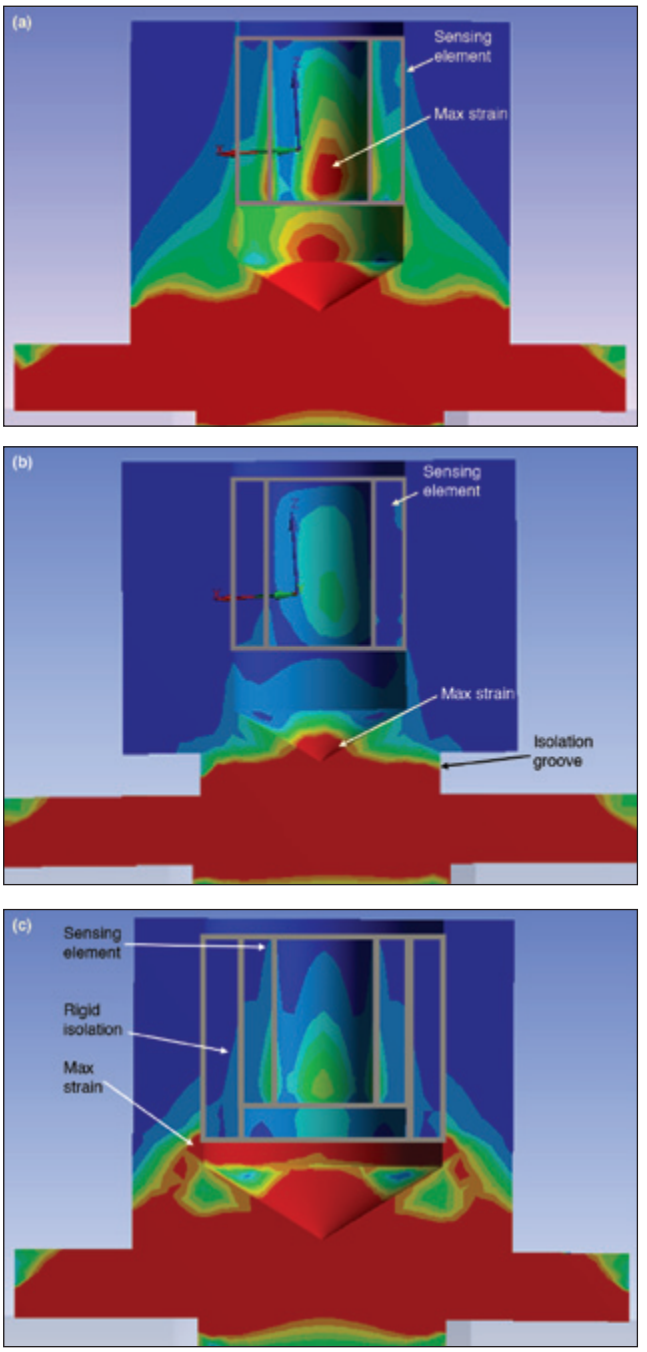

Figure 8. Effect of housing undercuts and rigid isolation on base strain: (a) standard housing, (b) undercut housing, (c) rigid, isolated housing.

Thermal properties of the isolation material must also be considered. Temperature changes can alter material properties of the isolator, which in turn will alter accelerometer performance. Thermal properties can constrain the useable temperature range of the accelerometer, since calibrations are typically performed at room temperature. As the temperature increases, the mechanical isolation material may become softer, lowering the accelerometer's resonance and lessening its flat frequency response (Figure 5a).

Additional design considerations can further protect the sensing element from base strain, improving accelerometer performance. During an extremely severe mechanical shock, some strain may still be transmitted through the mechanical isolator. Grooves or undercuts can be added to the accelerometer housing to concentrate the area of the base strain at a location away from the sensing element, reducing its affects. Figures 8a and 8b show a finite-element analysis of a housing before and after addition of an isolation groove. Note how the location of the maximum strain moves off of the sensing element when the isolation groove

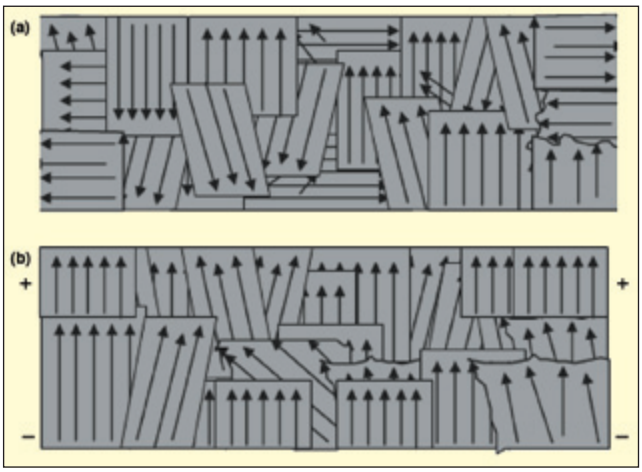

Figure 9. Poling of ferroelectric material: (a) With random dipoles; (b) after poling.

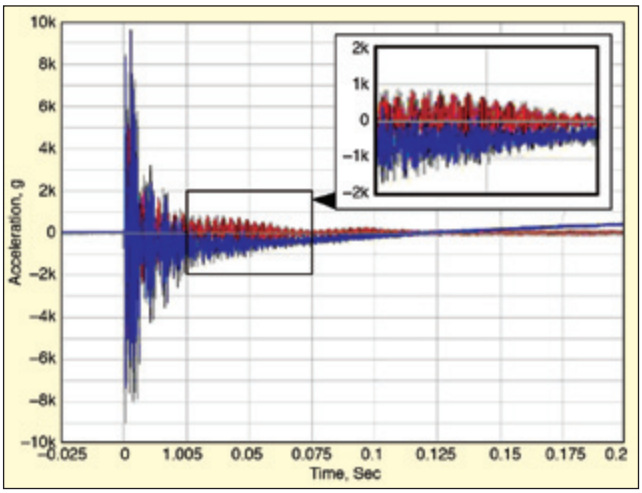

Figure 10. Accelerometer with baseline shift (blue) and without (red).

is added. Secondary rigid mechanical isolation can also be used to mitigate any base strain that has been transmitted through the primary mechanical isolator. Figures 8a and 8c show an FEA of an accelerometer with and without secondary rigid mechanical isolation. Note the reduction in strain on the sensing element with the addition of rigid isolation.

The type of piezoelectric material used in the sensing element is also an important design consideration. Ferroelectric ceramics are used in piezoelectric accelerometers because they have higher charge sensitivities than materials such as quartz. These materials are poled by high voltages during their manufacture to align their dipoles and induce a piezoelectric effect. Figure 9 shows the dipole alignment of a ferroelectric ceramic before and after poling.

Ferroelectrics can be susceptible to dipole realignment when overstressed, a phenomenon in which some of the dipoles switch back to random orientation. This realignment can cause the baseline shift or offset (called zero shift) shown in Figure 10. Mechanical isolation can help eliminate the chance for baseline shift or offset caused by overstressing a ferroelectric ceramic sensing element. Depending on the coercive forces between the dipoles, various ferroelectric ceramics display differing amounts of zero shift.

The effect of internal wiring is another important design consideration. The size and type of wire used within the sensing element can be critical to the proper functioning of the accelerometer. Large, single-strand wires can cause base strain by imparting side loads onto the element. Conversely, small, single-strand wires can fatigue more easily and result in a loss of output signal. Multistrand wires add flexibility to help prevent fatigue while increasing sensor durability.

Epoxy can be used to overcoat wires and to secure the various components of the sensing element; however, it must be used cautiously since it introduces other variables. Too much epoxy

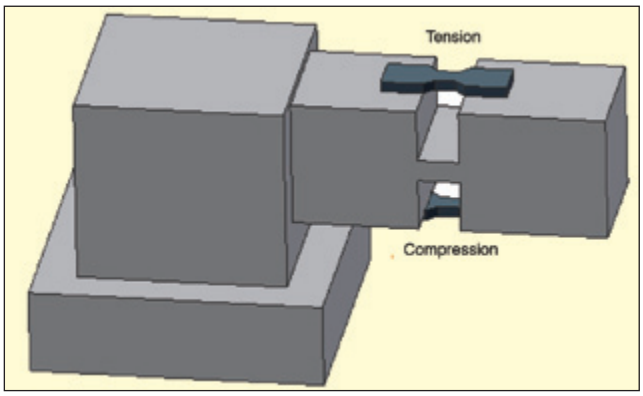

Figure 11. Silicon strain gages monitoring motion of cantilevered mass across slot.

can cause base strain by exerting side loads onto the element. Conversely, if not enough epoxy is applied, structural integrity may be compromised. Cleanliness of areas where epoxy is applied is critical to bonding. Contaminants, especially machining oils, can cause the epoxy to lose its bond. This can enable movement of the element components, resulting in zero shift and other signal output errors. Surface preparation (sandblasting, rough finish, etc.) all help promote epoxy adhesion.

In summary, the combined addition of mechanical isolation and electrical filtering has helped to make piezoelectric accelerometers more durable and reliable. These technologies, combined with other design lessons learned over the years, have helped reduce undesired stresses in accelerometer sensing elements, enhancing the probability of acquiring successful measurement of severe mechanical shock.

MEMS Technology. There are two principal reasons that strain gage technology can offer an attractive alternative to piezoelectric technology: 1) accurate response when integrating long-duration events (requiring flat frequency response to essentially zero Hertz); and 2) minimal zero shift. Metal wire and foil type strain gauges were initially used, but, as noted in Reference 4, piezoresistance technology began to be used in the 1970s, evolving into MEMS technologies in the 1980s. The piezoresistance property of silicon strain gages was found to be superior to that of foil gages, with an orders-of-magnitude higher gage factor provided by boron-doped silicon. The first sensor assemblies used thermally matched pairs of discrete doped silicon elements that were hand epoxied and hand wired to machined metal structures in a tension-compression bridge (see Figure 11).

The cost of this type assembly was high, and zero shift sometimes became an issue not due to the silicon gages but rather due to cracks or creep in the epoxy holding the gages to the structure. At times, even outright failure of the epoxy occurred. These weaknesses, i.e., both the application time and fragility of the epoxy, were addressed by the use of MEMS manufacturing techniques to simultaneously form the entire sensor structure for hundreds of sensors from a silicon wafer. The mechanical flexural elements were joined together as originally grown with gages predoped in the single crystal silicon.

The semiconductor processing allowed extreme miniaturization, enabling hundreds if not thousands of sensors to result for the same wafer processing cost, affording a potential price decrease in per-unit completed accelerometer. This miniaturization also provided the advantage of increased performance efficiency. Smaller structures have higher stiffness-to-weight ratios. This means the resulting sensors have lower sensitivities and higher resonant frequencies if all their parts are proportionately smaller. Since the trend over time in mechanical shock testing has been toward measuring increasingly higher acceleration levels, it was not a disadvantage that the new, smaller sensors had lower sensitivities and much higher resonances. One unexpected disadvantage was that the single crystal silicon had virtually no internal damping, unlike the natural damping properties (though small) attributable to the epoxies that held together the previous generation of manually assembled accelerometers (Figure 11).

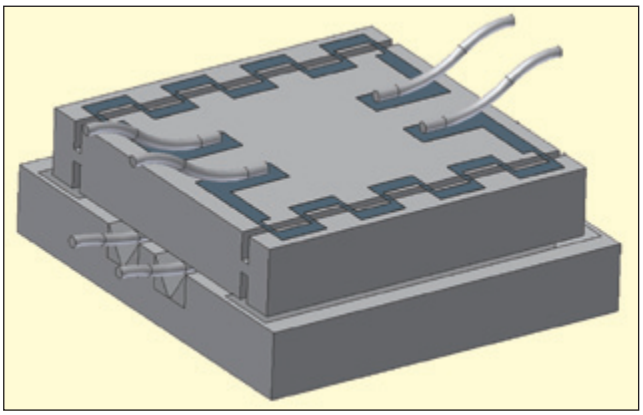

Figure 12. Early MEMS sensor developed for severe mechanical shock.

A depiction of the most successful of the earliest MEMS sensors is shown in Figure 12. Its size and efficient geometry provided extraordinarily high resonances, ranging from many hundreds of kilohertz to over a megahertz for the millimeter-sized chip. The sensor element was an assembly of a sensor chip attached to a pedestal. Although hundreds were made at a time from one wafer, each wafer needed to subsequently be diced, and these individual parts hand assembled. Because the design mimicked the arrangement of the manually assembled, discrete assembly of Figure 11, with tension gages above and compression gauges below, it required wire bonds on each side of the sensor chip. As noted previously, when completed the monolithic structure made of single crystal silicon possessed almost no internal damping.

As will be discussed subsequently, this lack of damping allowed very high levels of sensor resonant amplification. As one author (R. Sill) can attest as a member of that sensor development team, it was somewhat of a surprise to find that many shock inputs, even those with finite velocity change as opposed to pyrotechnic types, had sufficient energy in the megahertz range to excite its resonances. The result was frequent sensor failure from becoming overstressed. Therefore, some sensor damping was desired to reduce this resonant amplification.

Frictional dissipation of energy requires relative motion; however, the internal sensor displacements of the early MEMS shock accelerometers were practically at an atomic level. They were inadequate to facilitate any significant sensor damping. Although some early model, low-range, high-sensitivity piezoresistive sensors (made of large hand-assembled parts with relatively high displacements) used fluid damping with silicone oils, this was an impractical solution at extremely high g levels. In addition, the viscosity of oils was strongly affected by temperature, which meant the frequency response of sensors using oil damping was extremely temperature dependent. However, the viscosity of air is much less temperature dependent, which was exploited in the next generation of MEMS shock sensors.

Squeeze-film damping uses the motion of air "sloshing" between moving plates to dissipate energy. Similar to stiffness-to-weight ratios, as dimensions become very small the scale of viscous-to-inertial forces becomes larger. As dimensions between plates reduced to a few microns, early MEMS variable capacitance sensors for low g ranges could be optimally damped with just air. Key to that success was the comparatively large area of the plates of the capacitive elements and the very low stiffness of the flexures involved with these low g range devices.

Contrasted with the geometry of the sensor in Figure 12, the next generation of MEMS shock sensors developed at PCB was designed to utilize air damping. This was accomplished by increasing the area of the sensor's inertial mass, and decreasing the stiffness of its flexures. The section geometry of this new generation is shown in Figure 13. Both tension and compression gauges are more conveniently integrally doped on the top surface. The comparatively large cantilevers supporting the X-shaped inertial mass provide the area for damping. They are intentionally less efficient so the resonant frequency is as low as practical to allow adequate motion for squeeze film damping while still providing adequate sensitivity

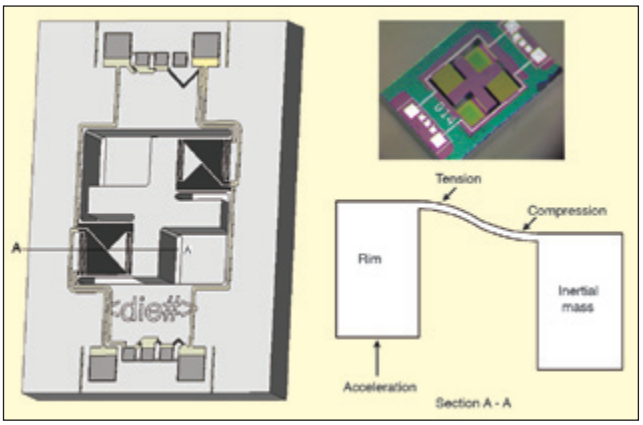

Figure 13. Core layer of PCB's MEMS lightly damped shock sensor.

Figure 14. PCB and legacy shock accelerometer on breakaway fixture.

and frequency response. Not shown are the lid and base layers that surround the core, providing the gap for squeeze-film damping and over-range stops and hermetic protection.

The initial version of PCB's MEMS sensor was designed for a full range of 20 kg. It was packaged in a variety of housings, including the Endevco 7270A's flat, two-screw package shown beside it in Figure 14. Because of its early development, identified previously to be 1983, the Endevco 7270 will subsequently be identified as the *legacy sensor*. The photograph shows the lightly damped PCB sensor prepared for a side-by-side comparison on a Hopkinson Bar with the packaged legacy sensor depicted in Figure 12. This "breakaway" fixture was placed on the end of the bar to allow free flight for comparison of zero shift of the PCB 3991A1020K with an identically ranged legacy sensor. Between this fixture and the end was placed a quartz plate with electrodes, to serve as a force gage reference. The test was performed by Dr. Danny Frew (then of Sandia National Laboratories) on the Hopkinson Bar at Purdue University.

Results of this Hopkinson Bar test are shown in Figure 15. Most noticeable is the enormous resonant response of the essentially undamped legacy sensor. The lower resonant frequency value of the lightly damped PCB sensor resulted in some small oscillations observed during the main pulse, which quickly dissipated, unlike the undamped legacy sensor response. It is now believed that relaxation of mounting screw preload releases elastic energy from the screws in bursts short enough to mimic the impulse sequence depicted in Figure 2.[6]

Good correlation during the initial pulse is shown among the three sensors in this Hopkinson Bar test (Figure 15). The PCB sensor had low-Q resonant amplification during this initial 10-kg pulse, and the 20-kg legacy sensor showed an extremely high Q (ringing) response after the breakaway fixture detached from the bar. After separation, zero shift is observed on the output of the monitoring (yellow) piezoelectric quartz disk. The initial test pulse of Figure 15 was carefully crafted to reduce high-frequency input in the Hopkinson Bar.

In contrast, another test was performed with the opposite intent – to maximize high-frequency input. A mechanical hammer test applied approximately 100 blows over a 2-second interval, with each blow generating peaks of approximately 10 kg as measured by the wideband data acquisition system (5 MHz sampling with 2.5 MHz anti-alias filters). The geometric arrangement of the sensors

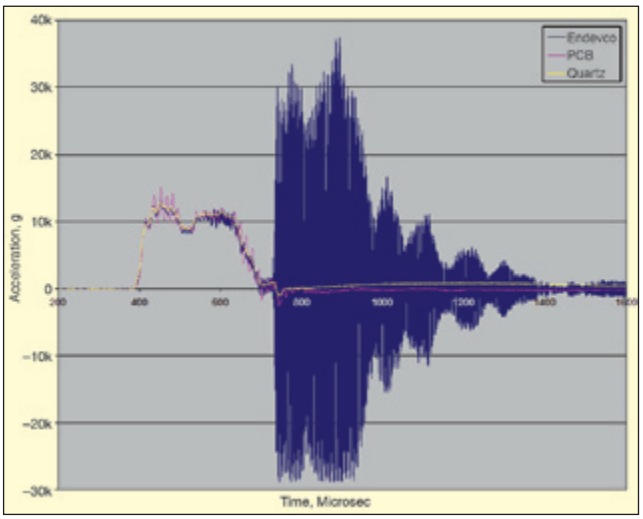

Figure 15. Comparative Hopkinson Bar with breakaway fixture sensor test results.

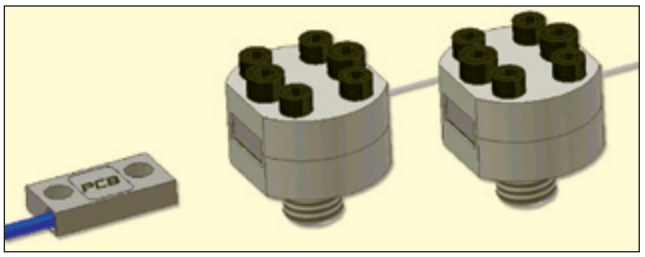

Figure 16. Relative size and separation of PCB and isolated legacy sensors used in testing.

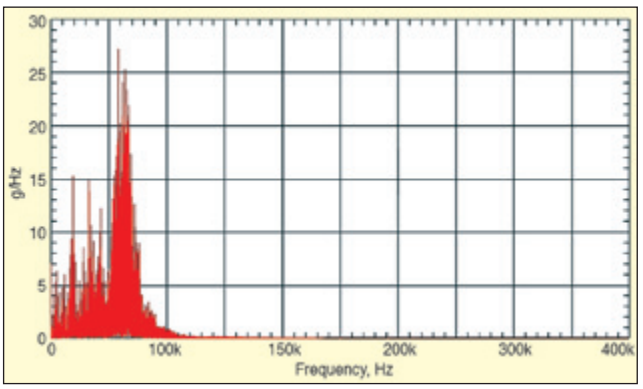

Figure 17. Representative FFT spectrum from PCB 20 kg sensor subjected to a 10 kg hammer blow.

tested is shown in Figure 16. This depiction shows the size and relative separation of the PCB sensor alongside two mechanically filtered legacy sensors that were on the same test specimen. The point of impact was near the sensors, in a direction normal to the mounting surface, and therefore parallel to the sensitive axis of all of the sensors. The mechanically filtered package is traditionally used to prevent sensor failure due to over-range from resonant amplification in the high-Q legacy sensor during explosive events and metal-to-metal impacts.

Figure 17 shows the resulting FFT spectrum from the PCB 20-kg sensor in Figure 16 when subjected to one of the 10-kg hammer blows. A more revealing view of the high-frequency components of the new sensor is shown and is discussed in a logarithmic plot of these same data in Figure 19.

Figure 18 shows the equivalent FFT spectrum from the undamped 20-kg legacy sensor in one of the isolated rubber mechanical mounts subjected to the same 10-kg hammer blow as the PCB sensor in Figure 17.

Comparing the spectra of Figures 16 and 17 as close as possible, note that both seem to match each other below about 20 kHz. The PCB sensor shows the amplified response of its lightly damped 65

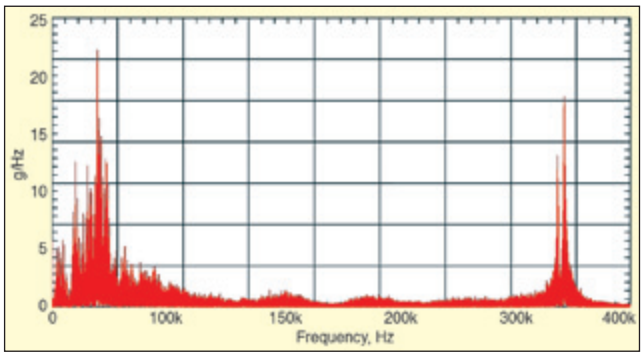

Figure 18. Comparative FFT spectrum from the legacy sensor.

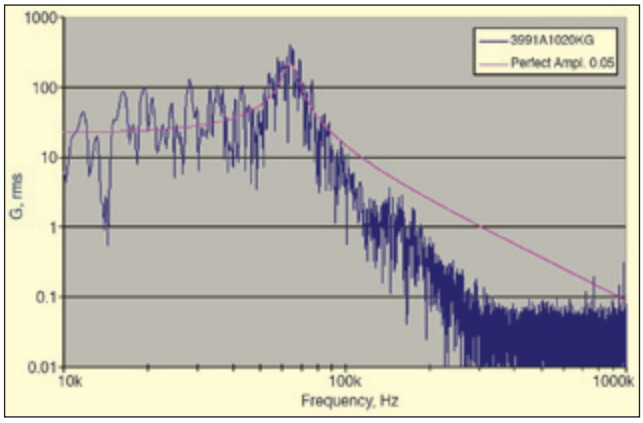

Figure 19. Logarithmic plot of PCB sensor data from Figure 17 with superposed single-degree-of-freedom, second-order system with a 65-kHz resonance and damping coefficient of ~0.05.

kHz resonance in Figure 17. The 30-40 kHz response associated with the resonance of the rubber isolation in the commercial legacy sensor M6 package is visible in Figure 18. The input is shown, remarkably, to include essentially white noise to 500 kHz or higher. High Q 380 kHz twin resonances associated with the 20-kg legacy sensor are illustrated despite the mechanical isolation. (A similar plot of a 60-kg legacy sensor displayed its resonances at 900 kHz.)

Figure 19 is an expanded logarithmic plot of the PCB sensor data from Figure 17. Overlaid is a theoretical single-degree-of-freedom response with a 65-kHz resonance and damping coefficient of ~0.05. Assuming that the energy in the hammer tests is fairly "white" (equal energy per unit frequency) as indicated by the response spectrum of the legacy sensor in Figure 18, the FFT magnitude of the output should approximately match the frequency response function of any sensor subjected to it. The roll-off of the new PCB MEMS sensor past the resonance in Figure 19 has a much steeper decline than a perfect single-degree-of-freedom response. This perhaps indicates that the squeeze film damping in the PCB sensor is more effective than expected. The conclusion that can be drawn from these data is that the light damping in the new MEMS sensors minimizes sensor overstress, thereby enhancing its ability to survive and measure severe mechanical shock measurements.

Laboratory Evaluation Techniques and Results

A well-designed shock sensor will accurately report on-axis acceleration while rejecting all extraneous electrical, mechanical, and environmental inputs as it is subjected to shock levels that would damage most ordinary sensors. In the field, these extraneous inputs will occur in combination. In the laboratory, acceptance tests are constructed to singly quantify the sensor's influence to each input and then impose reasonable acceptance limits. Many of the acceptance tests performed on shock accelerometers are similar to tests performed on "ordinary" vibration accelerometers and include: vibration sensitivity, frequency response, base strain, transverse sensitivity, temperature coefficient of sensitivity, inherent noise, and immunity to electromagnetic interference. The only challenge with these ordinary acceptance tests is the acquisition of the very low level signal output from a high-range, low-sensitivity shock

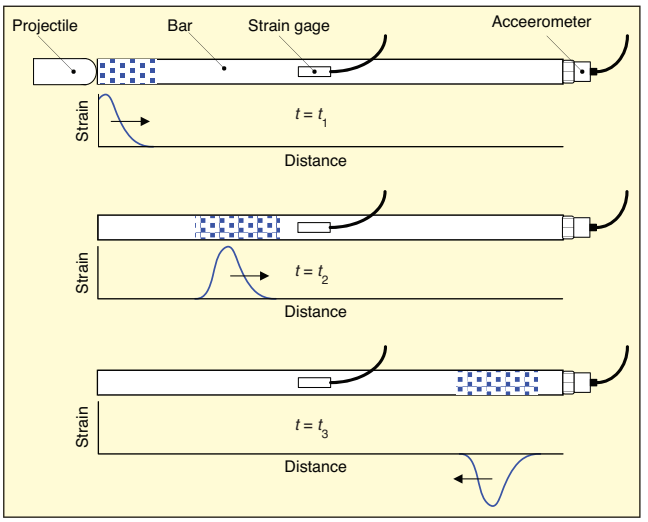

Figure 20. Three "snapshots" of propagating strain wave generated by projectile impact against a Hopkinson Bar.

accelerometer. Other parameters such as zero-shift, shock survivability, and linearity require testing on a Hopkinson Bar, a device capable of producing very high peak acceleration levels. In this section, theory and operation of the Hopkinson Bar is described followed by a discussion of the interpretation of Hopkinson Bar data.

Hopkinson Bar Acceptance Test System. The Hopkinson Bar test system can generate peak acceleration levels in excess of 100,000g. It consists of an instrumented titanium bar, a projectile and launch tube, signal conditioning, a PC-based data acquisition system and signal processing software.[7,8] The accelerometer under test is mounted on one end of the bar and reference strain gages are mounted near the mid-point of the bar. Impact of the projectile against the bar launches a strain transient whose shape approximates a half sine. Referring to Figure 20, impact of the projectile starts a compressive wave at time $t = t_1$, which propagates to the right at the speed c_o, the speed of a longitudinal wave in a solid. At time $t = t_2$, the leading edge of wave has reached the strain gage. The wave continues to the right until it is reflected at the accelerometer boundary as a tensile strain wave traveling to the left. The time $t = t_3$ is after the wave has reflected at the accelerometer boundary. The stress wave continues to propagate, reflecting back and forth until dissipative forces completely attenuate the wave.

Determining the bar's tip acceleration from the strain gage signal is straightforward. The velocity v at a point away from the ends of the rod is proportional to the reference strain ε_r:[2]

$$v(t) = c_o \varepsilon_r(t) \tag{1}$$

At the end of an unconstrained bar, the velocity is doubled and stress is zero. Thus, the reference velocity at the location of the accelerometer is:

$$v_r = 2c_o \varepsilon_r \tag{2}$$

The reference acceleration is found by differentiating the above expression:

$$a_r = 2c_o \frac{d\varepsilon_r}{dt} \tag{3}$$

Equation 3 is exact for reflection of an ideal one-dimensional strain wave in a long slender bar. This implies: dispersion and attenuation of the propagating stress wave is small, the stress wave is a simple 1D compression/tension wave, the compression wave is perfectly reflected at the accelerometer/bar boundary, and the stress-strain relationship is linearly elastic. These are reasonable assumptions given the frequency of interest, the size of the accelerometer, and the diameter of the bar in a typical accelerometer test. Furthermore, at PCB the relationship between strain and velocity is calibrated directly using a laser vibrometer rather than depending on the assumptions inherent in Equation 2.

A typical time waveform of a piezoceramic shock sensor mounted on a Hopkinson Bar is shown in Figure 21. Shown here are four reflections of the stress wave scaled to acceleration and integrated to velocity.

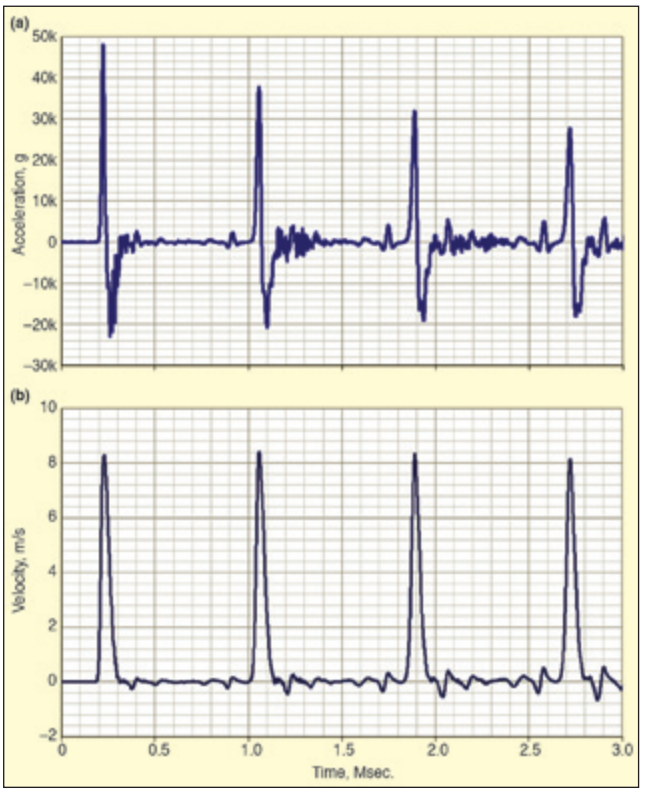

Figure 21. PCB Model 350C21 output, acceleration (a) and integrated velocity (b), from 50,000 g Hopkinson Bar test.

Interpretation of Test Results. In interpreting Hopkinson Bar acceptance test data, or any shock data for that matter, it is important to keep in mind that the sensor response depends on the input spectrum. One can have two shock inputs generated by a Hopkinson Bar with equal peak accelerations but have very different frequency spectra and damage potential. The sensor response and associated metrics of zero shift, frequency response, sensitivity, and other parameters depend implicitly on the shape of the shock waveform.

Ideally the Hopkinson acceptance test will exercise the sensor through its acceleration range with an acceleration spectrum representative of the field application. And equally important, the waveform must be consistently controlled so that every sensor tested is subject to the same shock conditions. In the Hopkinson Bar system, the waveform and peak level is controlled by maintaining control of a number of variables. The projectile material, hardness, diameter, length, and surface geometry have a strong influence on the frequency content. Projectiles must be monitored over time to ensure frequency spectrum does not change with use. Acceleration amplitude is controlled through projectile velocity, which is adjusted through air pressure in the launch tube.

The shock amplitude and frequency spectrum cannot be controlled independently. High-amplitude impacts are usually associated with higher frequency content. Increased high-frequency content at high amplitude can sometime be alleviated through the use of a mitigator (material placed between projectile and bar) or by changing the projectile/bar as amplitude is increased. Lastly, the data window chosen for processing the response will significantly influence the response metrics. Response can be based on a single pulse, a number of reflected pulses, or through the use of a "fly-away" mounting fixture, a portion of the first pulse.

Zero Shift. A zero shift is a change in the sensor's zero-g bias level while subject to shock. It is arguably the most important metric to be evaluated by the Hopkinson Bar test. It could be said that the ability to survive shock and report data without zero shift is what separates a shock sensor from an ordinary vibration accelerometer.

Every accelerometer manufactured by PCB that is classified as a shock sensor will undergo testing to demonstrate acceptable zero shift. For users of shock sensors, the potential problem is

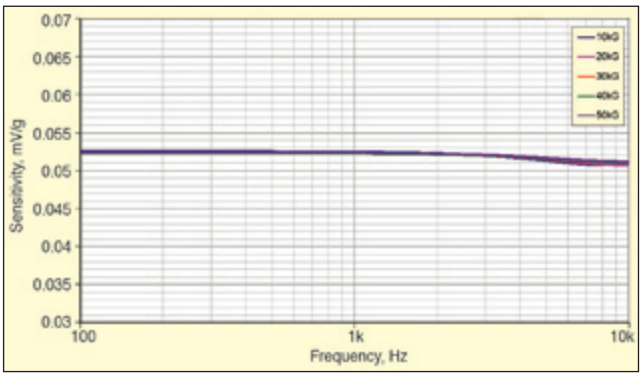

Figure 22. PCB Model 350C21 piezoceramic shock sensor frequency response (response at 5 levels from 10,000 to 50,000 g).

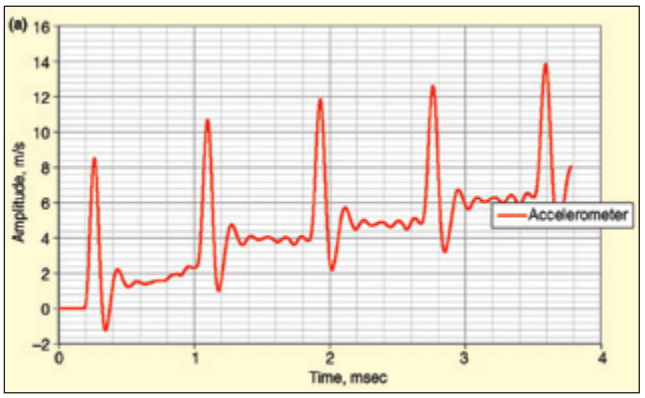

Figure 23. Shock sensor nonlinear response' (a) integrated signal does not return to zero and shows step-wise behavior; (b) frequency response changes with acceleration input; sensor is competitor's piezoceramic accelerometer with mechanical isolator.

that small shifts in the zero level will result in large errors when the time record is integrated to velocity or when transformed to a shock response spectrum. Threshold for acceptable zero shift is small and is most easily observed by integrating to velocity and a classic zero shift will be easily seen as a ramp in the velocity record. At PCB, acceptable value for zero shift is an internal metric, but it is very small and not usually stated in the specification. The value for zero-shift is expressed as the percent change in the bias referenced to the peak acceleration level.

Frequency Response. Accelerometer frequency response is usually and most accurately performed using sinusoidal vibration on a shaker against a back-to-back reference. In a shaker frequency response, the sensor is swept through the desired frequency range at relatively low acceleration levels ranging from 1 to 10 g. To obtain response while subject to high acceleration levels, shock excitation must be used. A frequency response from the Hopkinson Bar is obtained as follows:

- Accelerometer and strain data from the first pulse are obtained (data from subsequent reflections are ignored) and Fourier transforms are applied.
- The strain signal (proportional to velocity) is scaled to acceleration (g) in the frequency domain.

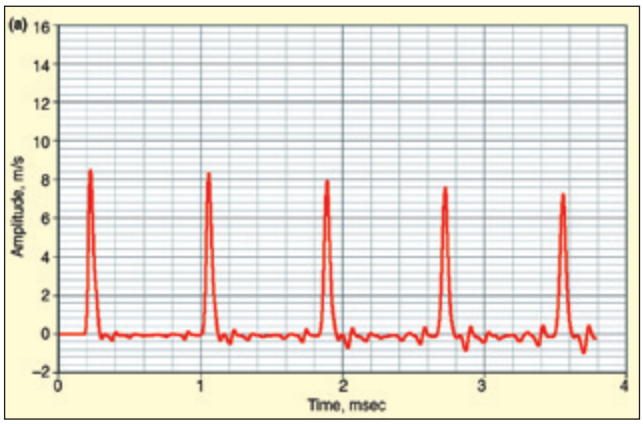

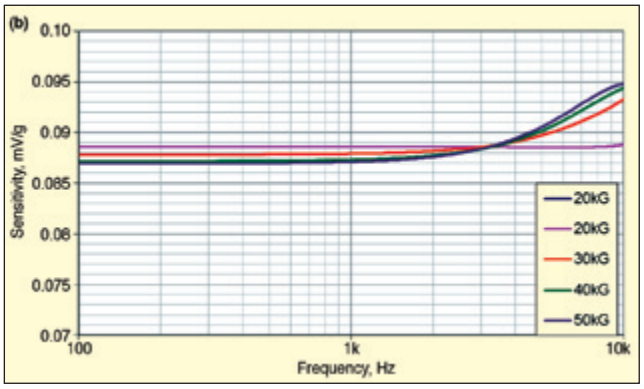

Figure 24. Linear fesponse from PCB Model 350D02 having mechanical isolation; (a) Velocity returns to zero after each impact; (b) Frequency response is consistent with acceleration level.

- The accelerometer sensitivity (mV/g) is obtained in the frequency domain as the ratio of the sensor output (volts) and reference acceleration (g).

An example of a shock sensor frequency response is shown in Figure 22. Responses were at obtained 5 shock impact levels from 10,000 to 50,000 g.

Sensitivity. Sensitivity (mV/g) is found by taking the ratio of the sensor under test and strain gage reference. This can be performed in the frequency domain as in Figure 22, or more commonly, it is found by peak picking in the time domain. To minimize error when using peak picking methods, it is important that the input does not contain high frequencies that would excite sensor resonance.

Nonlinearity. Nonlinearity is deviation of output from an expected linear input-output relationship. There are two common approaches to specify nonlinearity in shock sensors. Nonlinearity can be specified as the change in sensitivity with acceleration level (nonlinearity <2.5%/10,000 g). Alternatively nonlinearity can be expressed as maximum deviation from a best-fit straight line of the output as the sensor is shocked at 20% intervals up to full scale. For most piezoelectric and piezoresistive shock sensors the nonlinearity is small. An exception is that some older model mechanically isolated piezoelectric shock sensors can exhibit very large nonlinearity.

An example of such a sensor is shown Figure 23. Integrated to velocity, the time domain signal shows a series of steps that is the result of acceleration sensitivity being different in the positive direction compared to the negative. In the frequency domain, two effects of the nonlinearity can be observed. There is increase in sensitivity with g-level, and the resonant frequency of the mechanical isolator drops with acceleration level. Piezoelectric shock accelerometers with mechanical isolation can be manufactured with linear response as shown in Figures 24a and 24b. Here the velocity returns to zero after each impact and the frequency response is consistent with input level.

Lastly, Figures 25a and 25b show the Hopkinson Bar derived velocity and frequency response of a MEMS accelerometer PCB Model 3501A1260KG. Response is linear in that velocity returns to zero after each impact (Figure 25a), and sensitivity does not change

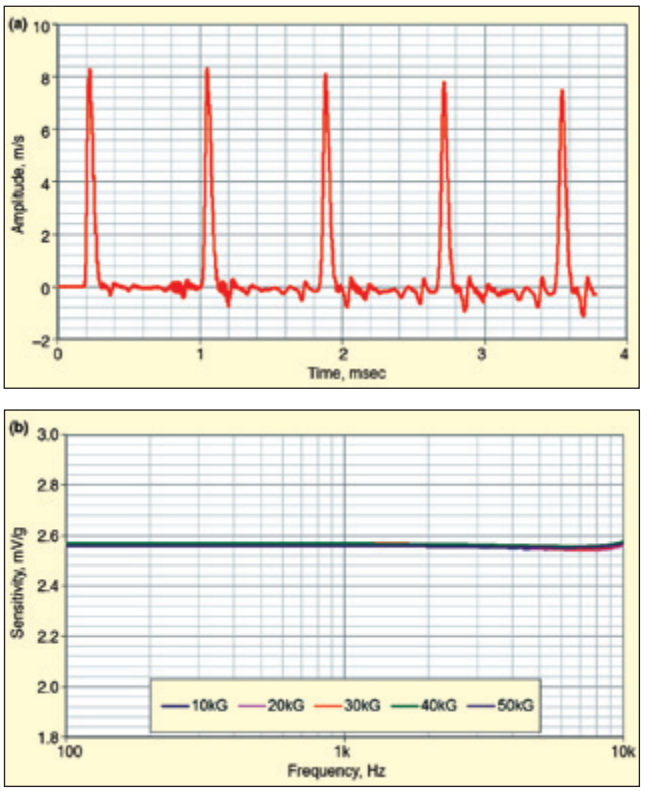

Figure 25. Linear response from PCB Model 3501A1260KG MEMS accelerometer; (a) Velocity; (b) Frequency response.

significantly with acceleration level (Figure 25b).

Field Performance

We have described the development and laboratory evaluation of both mechanically isolated piezoelectric and MEMS accelerometers. Every application that involves severe mechanical shock is different, and no single accelerometer solution is best suited for all. When zero shift of piezoelectric accelerometers occurs or accelerometer fragility becomes an issue, both of these technologies offer a potential solution.

Both mechanically isolated piezoelectric and MEMS accelerometers have been successfully used to characterize severe mechanical shock. Case studies are now presented to illustrate successful performance of both of these technologies under conditions of severe mechanical shock.

Penetration Tests with MEMS PR Accelerometers. Projectile penetration testing was performed at the U.S. Army's Engineering Research and Development Laboratory (ERDC) in Vicksburg, MS. Two ruggedized data recorders each with three-channel capability sampled the outputs of two triaxial configurations of both the lightly damped PCB Model 3991 and the legacy sensor. After the signals passed through 10-kHz anti-alias filters, the sampling rate was 75 kHz. The penetrator was launched at ~1440 ft/s into unreinforced, unconfined, 6000 psi concrete. It stopped after 33 inches of penetration and experienced a peak deceleration of 15 kg. The physical configuration is shown in Figure 26.

The waveforms at upper left and right of Figure 27 show results from the axially directed sensors during launch and impact, respectively. The transverse data for the launch are portrayed in the lower graphs, showing the largest rattle when leaving the barrel. Both legacy sensors in the transverse directions display zero-shift.[10] The erroneous data may be caused from improper mounting such as a loose mounting screw, lack of epoxy, or cable motion. All of these mounting errors can lead to post-shock base strain that manifests itself as zero shift.

Pyroshock Tests Comparing Mechanically Isolated Piezoelectric and MEMS Accelerometers. When working with live pyrotechnics on full-scale test articles is not practical, other methods to simulate defined shock response spectra have been developed. Pyroshock simulation techniques may be arranged into two categories: mechanically excited and pyrotechnically excited. Short-duration mechanical impacts on structures can produce a response similar to that produced by a pyrotechnic source. Mechanically excited simulations allow control of dominant frequencies up to about 10 kHz. For tests that require frequency content perhaps to 20 kHz, a pyrotechnically excited technique is usually more appropriate. In either technique, the use of piezoelectric shock accelerometers that lack mechanical isolation can create measurement errors in the velocity integral and SRS.

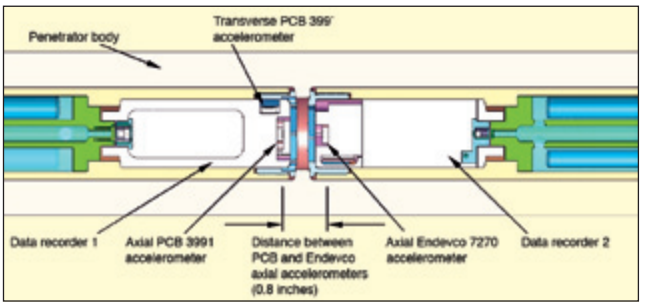

Figure 26. Placement of sensors and recorders.[10]

A question that always challenges the test engineer is which type of measurement sensor to select? Three sensors were compared in this test; mechanically isolated and electrically filtered piezoelectric 50-kg range PCB Model 350B02, 2% damped PCB MEMS 60-kg range Model 3501A1260KG, and the undamped MEMS legacy sensor in a 60-kg range. Figure 28a shows the location of the three sensors subject to a simulated pyroshock event. The impact to the subject test structure (Figure 28b) was achieved by a modified direct-fastening, powder-actuated system that is used to qualify components for spacecraft applications.

The mechanically isolated, piezoelectric, damped MEMS and undamped legacy sensor produced nearly equivalent test results. In this test, it was shown that all three can potentially be used in some severe mechanical shock applications, including pyroshock. Figures 29, 30 and 31 document the time response and the SRS of the tested accelerometers. As Figure 32 shows, all three sensor types show close correlation in their SRS responses up to 20 kHz. The case demonstrates that under controlled conditions, all three sensing technologies are suitable for severe mechanical shock measurements.

Pyroshock Tests with Mechanically Isolated and Nonisolated Piezoelectric Accelerometers. A pyroshock test pulse was performed on a tunable beam at MGA Research Corp., Akron, NY. Testing compared a mechanically isolated piezoelectric ceramic PCB 350C02 (50 kg) and a non-isolated piezoelectric ceramic PCB 350B21 (100 kg) shock accelerometer. The cantilever beam (Figure 33a) was clamped at one end of a massive base structure that imposed a nearly fixed-end condition on the beam. The shock accelerometers were mounted to the beam on a test plate located three inches apart and centered on the impact point. The sensors were impacted from below the beam by firing a projectile from an air gun beneath the beam. A close-up of sensor installation is shown in Figure 33b.

Figure 34 shows the shock acceleration time history. The 350C02 mechanically isolated piezoelectric accelerometer, considered the reference sensor for this test, shows a peak shock level of approximately 2400 g. The non-isolated accelerometer 350B21 produced peak levels up to 7000 g. The differences stem from the high Q factor at resonance for the 350B21. The two sensors differ in their waveform shape somewhat, since the sensors were not collocated. The benefit of mechanical isolation is clear in terms of removing high-Q-factor resonant amplification and the related measurement errors of overstating the peak acceleration of a shock pulse.

The associated SRSs in Figure 35 are rich with high-frequency content, evident by its plateau not occurring until near 10 kHz. The ideal max positive and negative SRS that results from the shock pulse should be symmetrical. Evaluating the SRS data for the 350C02, good symmetry is observed across the entire frequency range of 10 Hz to 10 kHz. The nonisolated PCB 350B21 is producing an offset (zero shift) as indicated by the rise in the SRS below

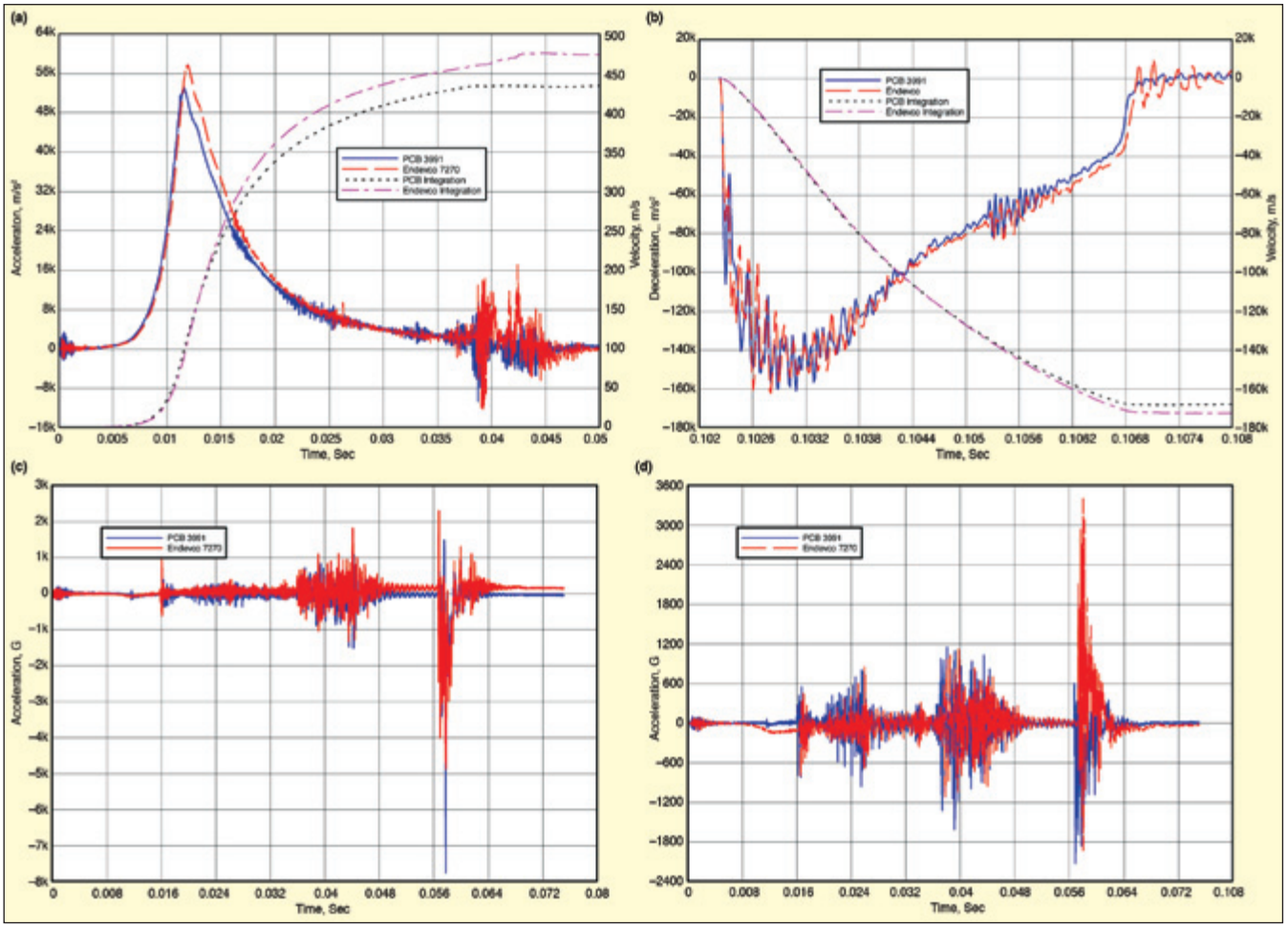

Figure 27. Comparative waveforms of triaxial configured sensors.

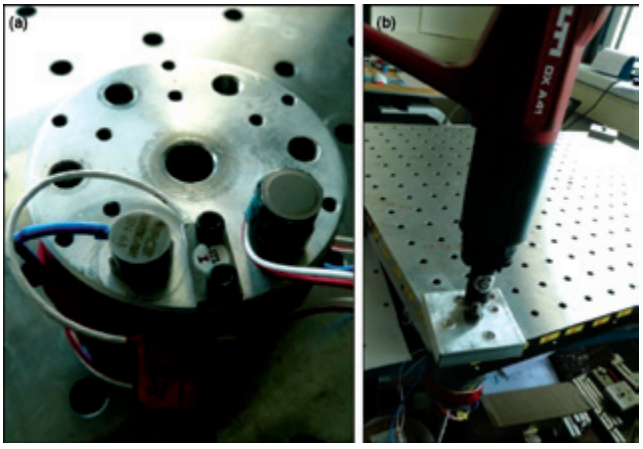

Figure 28. Metal impact test: (a) Test arrangement of shock sensors; (b) Fastener attachment during test.

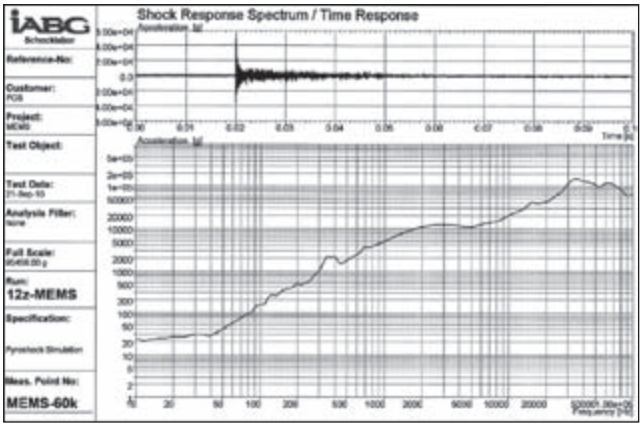

Figure 29. PCB 3501A1260KG DC coupled, time and SRS.

100 Hz. The isolated piezoelectric appears to provide very good results with positive and negative symmetry, and we may conclude that isolation is required in piezoelectric accelerometers for severe mechanical shock.

Both mechanically isolated and filtered and MEMS sensors have displayed the capability to measure severe mechanical shock. The data sets provided from real-world applications show successful application of isolated and LP-filtered piezoelectric accelerometers as well as MEMS accelerometers. The successful inclusion of a small amount of damping in MEMS accelerometers is improving their performance in severe shock environments. No two technologies will perform the same in every application due to the uniqueness of the individual environments. In addition to considering the basic accelerometer sensing technology in every application, detailed attention has to be paid to proper accelerometer mounting, cable/connector interface and assembly, cable tie-down, and more before a successful measurement can be initiated through the remainder of the measurement system.

Conclusions

The measurement of severe mechanical shock has many associated challenges.

- The mechanical shock environment typically has significant motion in six degrees of freedom. In early time (near $t = 0$), this motion is incapable of adequate modeling and therefore lacks definition.
- Extremely high frequencies accompany severe mechanical shock, and these high frequencies typically excite the resonant frequency of the accelerometer. As a result, the accelerometer can easily be over-ranged or driven nonlinear due to this resonance excitation.
- In highly energetic environments, accelerometers can be subjected to significant levels of kinetic energy.
- Base strain can be a problematic, extraneous input to the accelerometer. Other harmful environments may co-exist (thermal transients, ionized gases, etc.).

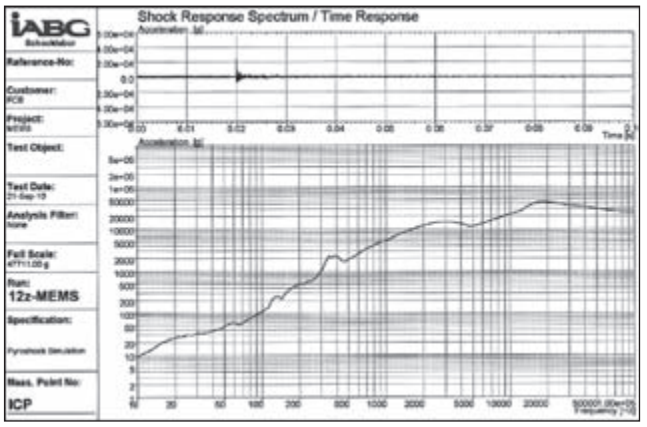

Figure 30. PCB 350B02 ICP® coupled, time and SRS.

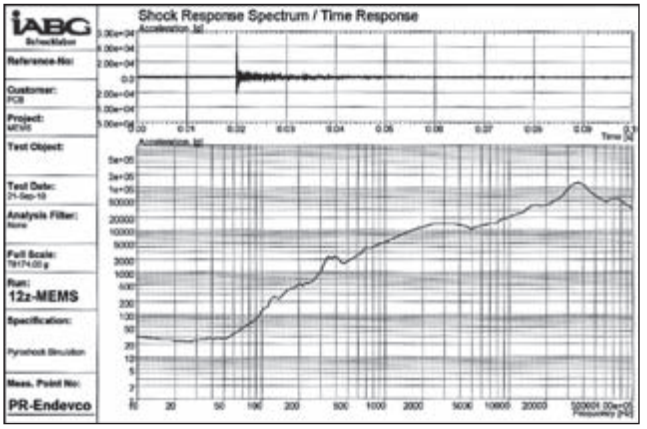

Figure 31. Legacy sensor DC coupled, time and SRS.

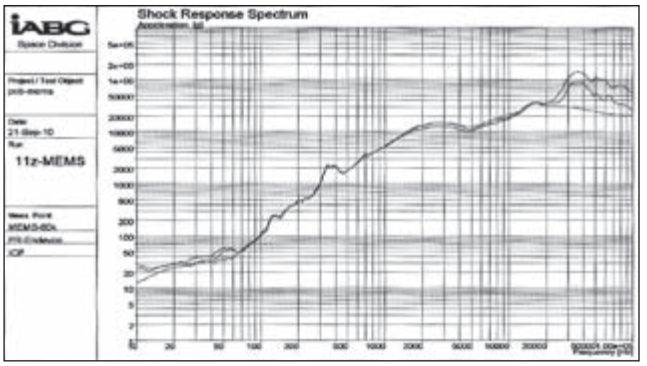

Figure 32. SRS overlay of all three sensors.

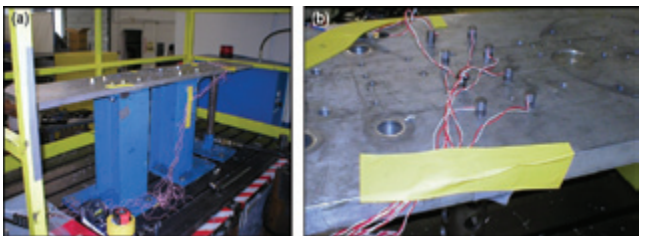

Figure 33: Pyroshock test setup at MGA[11]: (a) Pyroshock tunable beam; (b) Sensor installation on beam.

- Cable-induced noise is always a potential concern.
- Over the years, research and experience has documented that under severe mechanical shock loading ferroelectric ceramic accelerometers often display a baseline shift or offset from their initial zero at shock termination. Mechanical isolation of ferroelectric ceramic accelerometers, coupled with an internal two-pole filter available in an ICP circuit is allowing piezoelectric accelerometers to operate successfully at higher g levels than were previously achievable. Good design practices are allowing their elastomeric isolation materials to perform in a dynamically linear fashion within the accelerometers.
- As an alternative technology to piezoelectric accelerometers, a new generation of MEMS shock accelerometers has been evolved. As opposed to existing legacy MEMS sensors, these designs incorporate: squeeze-film damping, over-range stops, and hermetic protection.
- To investigate their performance, accelerometers designed to measure severe mechanical shock are subjected to very high acceleration levels on a Hopkinson Bar. Parameters evaluated include zero shift, shock survivability, and linearity.
- In some situations, the frequency environments associated with severe mechanical shock may be so expansive, the acceleration levels so high, or the other directional inputs so severe that successful measurements simply cannot be obtained. In addition, there is no single accelerometer design that is a "magic bullet" optimum for every measurement challenge. Advances in state-of-the-art accelerometer design have resulted in improved technology options for severe mechanical shock. These technologies have been shown to be raising the limits as to the types and levels of accelerations that can be successfully measured.

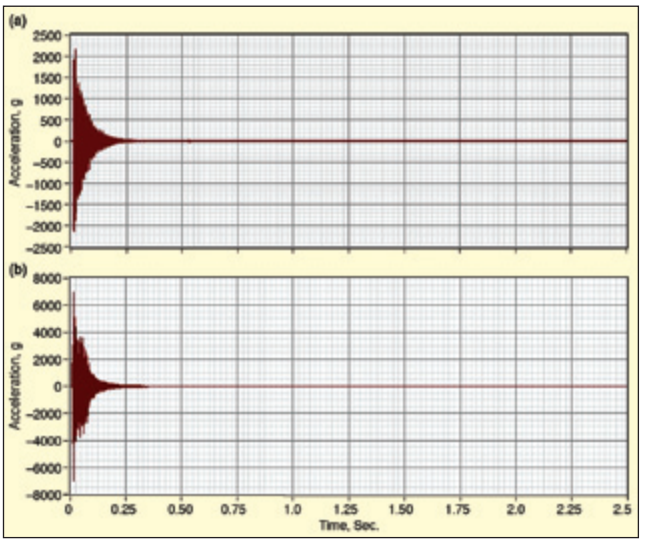

Figure 34. Acceleration data from tunable beam test; (a) 350C02; (b) 350B21 .

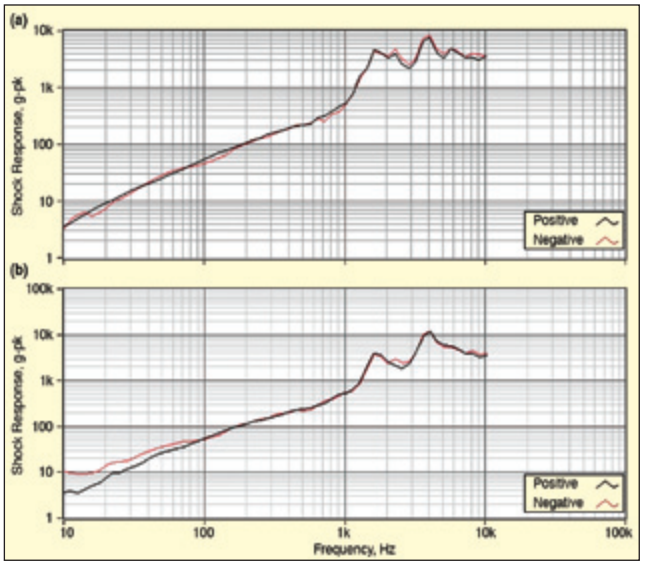

Figure 35: SRS data from tunable beam Test (a) 350C02; (b) 350B21.

References

1. MIL-STD-810G, Department of Defense Test Method Standard: Environmental Engineering Considerations and Laboratory Tests, October 31, 2008.
2. IEST-RP-DTE032, Pyroshock Testing Techniques, October 2009.
3. NASA-STD-7003, Pyroshock Test Criteria, December 20, 2011.
4. Walter, Patrick L. "Lessons Learned in Applying Accelerometers to

Nuclear Effects Testing," *The Shock and Vibration Digest*, Volume 15, Number 6, IOS Press, November 2008.
5. Plumlee, Ralph H., "Zero-Shift in Piezoelectric Accelerometers," Sandia National Laboratories Research Report, SC-RR-70-755, March 1971.
6. Dodson, Jacob C., Coker, Jordan, Glikin, Neil, Wolfson, Janet C., Foley, Jason R., "Energy Transmission Across Threaded Preloaded Interfaces," *Proceedings 83rd Shock and Vibration Symposium (SAVE)*, New Orleans, LA, Nov 4-8, 2012.
7. Sill, R, "Shock Calibration of Accelerometers at Amplitude to 100,000 *g* Using Compression Waves," *Proceeding of the 29th International Instrument Symposium,* Albuquerque, NM, pp. 503-516, 1983.
8. Dosch, Jeffrey, Jin, L., "Hopkinson Bar Acceptance Testing for Shock Accelerometers," *Sound and Vibration*, Vol. 33, No. 2, pp. 16-21, February 1999.
9. Davies, R. "A Critical Study of the Hopkinson Pressure Bar," *Philosophical Transaction, Series A.*, Royal Society of London, Vol. 240, pp 352-375, 1948.
10. Sill, R. "Field Evaluations of a Damped MEMS Shock Sensor," 79th Shock and Vibration Symposium, Orlando, FL, 2008.
11. Photo courtesy of MGA Research Corp., Akron, NY.

The author may be reached at: p.walter@tcu.edu.